Rehinging biflagellar locomotion in a viscous fluid

Saverio E. Spagnolie*
Courant Institute of Mathematical Sciences, New York University, New York, New York 10012, USA
and Department of Mechanical and Aerospace Engineering, University of California at San Diego, 9500 Gilman Drive, La Jolla, California 92093, USA

(Received 17 August 2009; published 30 October 2009)

A means of swimming in a viscous fluid is presented, in which a swimmer with only two links rotates around a joint and then rehinges in a periodic fashion in what is here termed *rehinging locomotion*. This two-link rigid swimmer is shown to locomote with an efficiency similar to that of Purcell's well-studied three-link swimmer, but with a simpler morphology. The hydrodynamically optimal stroke of an analogous flexible biflagellated swimmer is also considered. The introduction of flexibility is found to increase the swimming efficiency by up to 520% as the body begins to exhibit wavelike dynamics, with an upper bound on the efficiency determined by a degeneracy in the limit of infinite flexibility.

DOI: 10.1103/PhysRevE.80.046323 PACS number(s): 47.63.Gd, 47.63.mf

I. INTRODUCTION

Reciprocal motions are not effective means of locomotion in highly viscous fluids, a result known as the Scallop theorem, which is so named because of the sole reciprocal motions available to a scallop (opening and closing) [1]. For example, the flapping of a rigid wing is reciprocal and has been shown to generate locomotion only if the frequency Reynolds number is above a critical value of order one [2–4]. Given such limitations on reciprocal motions, microorganisms locomote by nonreciprocal undulations, frequently driving themselves with flagella, cilia, or other obtrusions. An overview of ciliary and flagellar fluid mechanics is provided by Lighthill [5] and excellent reviews are presented in [6,7].

Swimming at low Reynolds numbers has recently been a topic of active interest, in part due to an improved ability to visualize micro-organismic motility [8–10], but also due to the potential for engineering solutions in the field of medicine. An understanding of simple and effective means of propulsion at very small scales may soon lead to the development of microswimmers, which can be used for drug delivery, image transmission, and minimally invasive surgical techniques [11]. Biomimetic swimming devices powered by mechanical "flagella" have recently been constructed and studied [12–15]. However, such engineered microswimmers need not be biologically inspired. Other possible swimmers that have been proposed include a three-mass system [16], a deformable two-dimensional (2D) loop [17], a surface-treadmilling torus [1,18,19] or ellipsoid [20], and Purcell's three-link swimmer [1]. The last-named is constructed by connecting three rigid links by two hinges, leaving two free ends. The body achieves a positive mean velocity by rotating the two outer links in a nonreciprocal pattern.

Jung *et al.* [21] showed by experiment and numerical simulation the existence of periodic sedimentation orbits for a wide range of body types. These periodic orbits hint at a new idea for a simple means of locomotion in highly viscous fluids, one which is in some sense simpler than the mechanisms mentioned above and should provide excellent path-stability properties over long distances: a swimmer with only two links, alternatingly connected by two different hinges in what will be referred to as *rehinging locomotion*. The basic motion is illustrated in Fig. 1(a) for a body with link lengths L. The two links rotate around a hinge on the left (steps 1 and 2), and the connection joint between them moves to the right. Eventually the free ends come into contact (3), at which point they lock together while the original hinge unlocks (4). The previously connected ends become the new free ends, and steps (1)–(4) are repeated.

In this paper the swimming dynamics of a rehinging body is considered. The effects of flexibility are explored by increasing the number of links in a more general rehinging biflagellar swimmer, as illustrated in Figs. 1(b) and 1(c). The addition of flexibility is shown to increase the swimming efficiency by up to 520% as the body begins to exhibit wavelike dynamics, with an upper bound on the efficiency determined by a degeneracy in the limit of infinite flexibility.

II. KINEMATICS AND FLUID-BODY INTERACTION

We present the equations of motion for the general biflagellar swimmer of Fig. 1(b), of which the two-link rehinging swimmer is a simple (rigid) subset. The upper filament is labeled S_1 and we assume that the lower filament S_2 is at all times the mirror image of S_1 about the x axis. Both filaments have length L, and the connecting joint, or hinge, is assumed to be massless. The position of a point on S_1 is denoted by

$$\mathbf{X}(s,t) = x_0(t)\hat{x} + \mathbf{x}(s,t) = [x_0(t) + x(s,t)]\hat{x} + y(s,t)\hat{y}, \quad (1)$$

where $s \in [0,L]$ is the arc length, t is time, $x_0(t)$ is the horizontal position of the hinge, and $\mathbf{x}(s,t) = x(s,t)\hat{x} + y(s,t)\hat{y}$ describes the body shape. A period of motion is denoted by $t = T$. The body velocity at a material point $\mathbf{X}(s,t)$ is

$$\mathbf{X}_t(s,t) = U_0(t)\hat{x} + \mathbf{x}_t(s,t), \quad (2)$$

where $U_0(t) = \dot{x}_0(t)$ is the horizontal velocity of the connecting hinge. The assumption of symmetric flagellar motion for

*http://maeresearch.ucsd.edu/spagnolie/

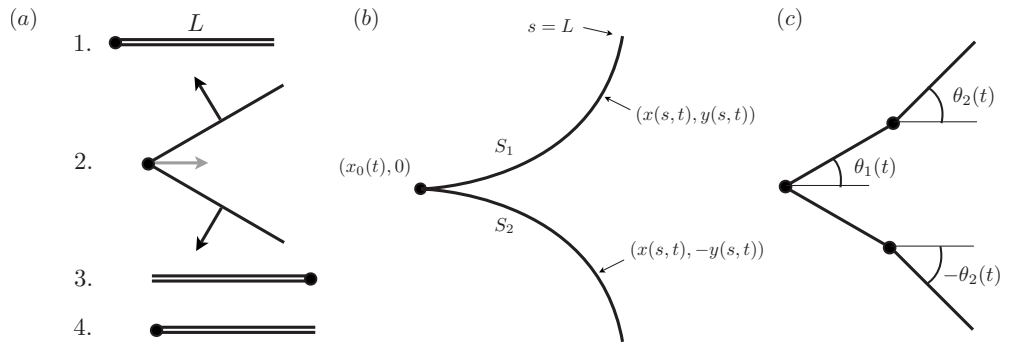

FIG. 1. (a) A rehinging two-link swimmer undergoes one period of motion and travels a distance of approximately $L/4$. After each stroke the (massless) hinge slides from one end to the other, and the motion repeats. (b) The general up-down symmetric biflagellar swimmer and parametrization. (c) A four-link swimmer ($M=2$).

the filaments S_1 and S_2 ensures that the hinge's vertical velocity and the net body rotation are always zero. The initial and final body positions (before rehinging) require [see Fig. 1(a)]

$$\mathbf{x}(L,0) = x(L,0)\hat{x} + y(L,0)\hat{y} = L\hat{x}, \tag{3}$$

$$\mathbf{x}(L,T) = x(L,T)\hat{x} + y(L,T)\hat{y} = -L\hat{x}. \tag{4}$$

The body is assumed to locomote in the Stokesian regime, where viscous dissipation dominates any inertial effects. The fluid-body interactions are modeled using the local resistive force theory developed by Gray and Hancock [22]. Resistive force theory relates the local fluid force per unit length and the local fluid-body velocity (equivalent by the assumption of a no-slip boundary condition). In the classical theory, the force per unit length $\mathbf{f}(s,t)$ relates to the local velocity at leading order in the body aspect ratio $\epsilon \ll 1$ via

$$\mathbf{f}(s,t) = \frac{2\pi\mu}{\ln(2/\epsilon)}(2\mathbf{I} - \hat{\mathbf{s}}\hat{\mathbf{s}}^T)\mathbf{X}_t(s,t), \tag{5}$$

where $\hat{\mathbf{s}} = (x_s, y_s)$ is the unit tangential vector on S_1. With no external forcing, the dynamics are thus set by conditions ensuring zero net force and zero net torque on the body at all times,

$$\int_0^L \mathbf{f}(s,t)ds = 0, \quad \int_0^L \mathbf{x}(s,t) \times \mathbf{f}(s,t)ds = 0. \tag{6}$$

The fluid stress is decomposed as $\mathbf{f}(s,t)|_{S_1} = \mathbf{f}(s,t) = f_1(s,t)\hat{x} + f_2(s,t)\hat{y}$ on S_1, and $\mathbf{f}(s,t)|_{S_2} = f_1(s,t)\hat{x} - f_2(s,t)\hat{y}$ on S_2 by symmetry. Writing the horizontal component of force in terms of the velocity in Eq. (2), we have

$$f_1(s,t) = \frac{2\pi\mu}{\ln(2/\epsilon)}\{(2 - x_s^2)[U_0(t) + x_t] - (x_s y_s)y_t\}. \tag{7}$$

The zero net vertical force and zero net torque conditions are satisfied automatically by the body's up-down symmetry. The only remaining constraint on the motion, therefore, is zero net horizontal force,

$$\int_0^L f_1(s,t)ds = 0. \tag{8}$$

Inserting Eq. (7) into the above yields the translational velocity of the connecting hinge,

$$\int_0^L (2 - x_s^2)[U_0(t) + x_t] - (x_s y_s)y_t ds = 0 \tag{9}$$

$$\Rightarrow U_0(t) = \frac{\int_0^L (x_s y_s)y_t - (2 - x_s^2)x_t ds}{\int_0^L (2 - x_s^2)ds}. \tag{10}$$

Hence, a prescription of the body shape $\mathbf{x}(s,t)$ is sufficient to set the swimming velocity $U_0(t)$, and time enters only as a parameter. Using Eq. (10), the velocity of the rehinging two-link swimmer is found by setting $x = s\cos[\theta_1(t)]$ and $y = s\sin[\theta_1(t)]$. Inertia plays no role in the low Reynolds number regime, so that opening and/or closing in one direction faster than the other has no effect on the net motion; only the body geometry is important. Without loss of generality the connection angle between S_1 and S_2 is assumed to grow linearly in time, $\theta_1(t) = \pi t/T$. To compute the distance traveled after one stroke, we monitor $s = L/2$ (the midpoint of S_1), the sole point on S_1 that does not change spatial position upon body rehinging. Using Eq. (10), the hinge velocity is

$$U_0(t) = \frac{\pi L}{T}\frac{\sin(\pi t/T)}{2 - \cos^2(\pi t/T)}, \tag{11}$$

so that the distance traveled by the midpoint after one stroke, ΔX, is

$$\Delta X = \int_{t=0}^{t=T} U_0(t) + x_t\left(\frac{1}{2}, t\right)dt = \sqrt{2}L\tanh^{-1}\left(\frac{1}{\sqrt{2}}\right) - L \approx \frac{L}{4}. \tag{12}$$

Hence, the body travels one body length in approximately four periods of rehinging motion. The distance traveled by the connecting hinge ($s=0$) prior to rehinging, approximately $5L/4$, is also derived by Becker *et al.* [23] as a launching point to study Purcell's three-link swimmer. On the scale of a spermatozoan, $L \sim 10^{-2}$ cm, $T \sim 1$ s, and the maximal hinge velocity is $\|U_0\|_\infty = \pi L/(2T) \sim 10^{-2}$ cm/s [25].

III. OPTIMIZING THE GENERAL M-LINK SWIMMER

To consider the effects of increased flexibility, we consider bodies with M links on each flagellar filament S_i (i

$=1,2$). A four-link rehinging swimmer ($M=2$) is illustrated in Fig. 1(c). The kth link is oriented with angle $\theta_k(t)$ to the horizontal, and the upper-half of the body (S_1) is defined piecewise linearly,

$$\mathbf{x}_k(s,t) = \mathbf{x}_{k-1}\left(\frac{L}{M},t\right) + \left(s - \frac{(k-1)L}{M}\right) \times \langle \cos\,\theta_k(t), \sin\,\theta_k(t)\rangle \quad \left(\frac{(k-1)L}{M} \le s \le \frac{kL}{M}\right), \tag{13}$$

with $\mathbf{x}_0(L/M,t)=0$, and $k=1,2,\ldots,M$. The initial and final conditions for a single stroke are written in terms of the angles as $\theta_k(0)=0$, $\theta_k(T)=\pi$ for all k. Each of the angles is expanded in a Fourier basis in time,

$$\theta_k(t) = \pi\left(\frac{t}{T}\right) + \sum_{n=1}^{\infty} a_{k,n} \sin\left(\frac{n\pi t}{T}\right). \tag{14}$$

A deviation angle is defined as $\bar{\theta}_k(t)=\theta_k(t)-\pi(t/T)$. In the Stokesian regime, time can always be re-scaled so that $\theta_1(t)=\pi t/T$ without loss of generality ($a_{1,n}=0$). The case $a_{k,n}=0$ for all k corresponds to a broad flat stroke, equivalent to the only possible stroke in the two-link case ($M=1$). The expression for the angles $\theta_k(t)$ is truncated by keeping only the first N Fourier modes.

Using Eq. (10) as before, an expression for the swimming velocity may be derived,

$$U_0(t) = \left(\frac{L}{M}\right)\frac{\sum_{k=1}^{M} P_k}{2M - \sum_{k=1}^{M}\cos^2[\theta_k(t)]}, \tag{15}$$

where

$$P_k = \sin[\theta_k(t)]\theta_k'(t) + \sum_{j=1}^{k-1}[\cos\,\theta_k(t)\sin\,\theta_k(t)\cos\,\theta_j(t) + \{2-\cos^2[\theta_k(t)]\}\sin\,\theta_j(t)]\theta_j'(t). \tag{16}$$

Equation (13) is used along with the above expression for the swimming velocity to determine the force $\mathbf{f}(s,t)$ via Eq. (5). The hydrodynamic efficiency is defined using a measure $\mathcal{E}$, which has been used by many authors, a ratio of the power required to drag the swimmer in its straightened configuration (two filaments of length L) at its average speed to the average power exerted mechanically against viscosity over a single stroke ([23–26]),

$$\mathcal{E} = \left[\frac{4\pi\mu L V^2}{\ln(2/\epsilon)}\right] \Big/ [2\langle\Phi\rangle], \tag{17}$$

$$\Phi(t) = \int_0^L \mathbf{x}_t(s,t)\cdot\mathbf{f}(s,t)ds = \frac{2\pi\mu}{\ln(2/\epsilon)}\int_0^L \mathbf{x}_t(s,t)\cdot(2\mathbf{I}-\hat{\mathbf{s}}\hat{\mathbf{s}}^{\mathbf{T}})[U_0(t)\hat{x}+\mathbf{x}_t(s,t)]ds. \tag{18}$$

$\Phi(t)$ is the mechanical power applied by each filament S_i, $2\langle\Phi\rangle$ is the total time-averaged power exerted over a full stroke, and V is the average horizontal velocity of the midpoint $s=L/2$, $V=\langle U_0(t)\rangle - L/T$. The efficiency so defined is independent of the aspect ratio ϵ.

To compute the efficiency for an arbitrary stroke form, the mechanical power and swimming velocity are determined at times corresponding to Gaussian quadrature nodes on the interval $t\in[0,T]$ (see [27]). Time averages of the quantities necessary to compute the efficiency are in this way determined to high accuracy with very few time steps. The hydrodynamically optimal body morphology is found by using an SQP Quasi-Newton line search method built into the MATLAB optimization toolbox. The coefficients $a_{k,n}$ are the adjustable degrees of freedom, and are determined numerically such that the efficiency $\mathcal{E}$ is maximized. Constraints on the Fourier modes were included to avoid solutions in which the body intersects itself. Any station s crossing the x axis ensures an intersection event due to the mirror symmetry of the body, so to avoid such an event we required

$$\sum_{i=1}^{m}\sin[\theta_k(t)] > 0 \tag{19}$$

for all $m\in[1,M]$ and for each time t at which the velocity and efficiency were computed. This constraint was found to be sufficient in practice. Many initial guesses were inserted into the optimization search to increase the likelihood that a global optimum was found, but the results reported here were found to be robust.

Results

Under the efficiency measure $\mathcal{E}$ defined above, the two-link (rigid) swimmer is found to be less efficient than some other forms of Stokesian locomotion; Eqs. (10) and (17) return an efficiency of $\mathcal{E}=.0165$. This compares unfavorably to more complicated structures such as the undulating filaments and helical swimmers ($\mathcal{E}=0.086$) presented in [24]. However, Purcell's three-link swimmer as studied in [23] has an efficiency of $\mathcal{E}=0.007$, and further optimizations of the Purcell stroke by Tam and Hosoi [26] and then Raz and Avron [28] have allowed for efficiencies in extreme cases up to $\mathcal{E}=0.0208$. The rehinging two-link swimmer is on par with this similar means of locomotion, but is far simpler in structure than the Purcell swimmer.

The efficiency increases dramatically when the numbers of links and Fourier modes for each angle $\theta_k(t)$ are increased. The optimal stroke in the four-link case ($M=2$) using the first $N=80$ Fourier modes is shown in Fig. 2(a), along with a plot of the deviation angle $\bar{\theta}_2(t)$ as a function of time. Arrows indicate the direction of motion of the hinge. The outer seg-

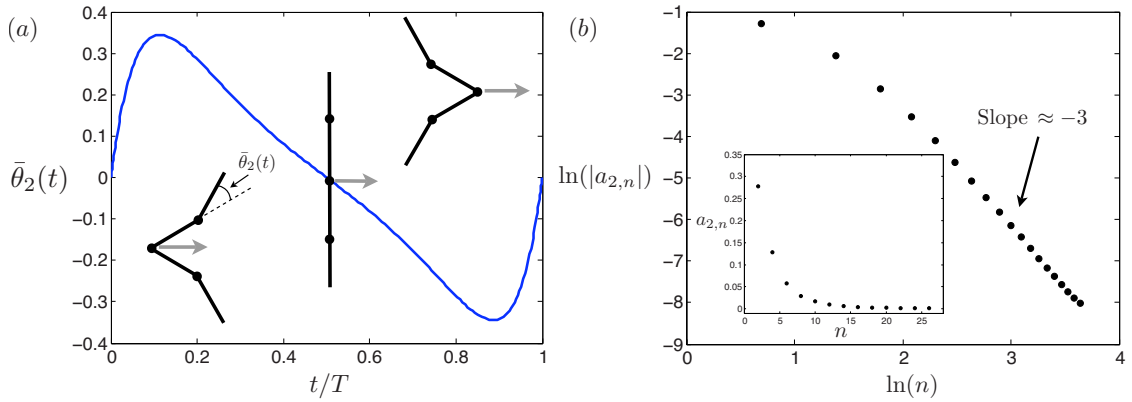

FIG. 2. (Color online) (a) The optimal profile of the deviation angle $\bar{\theta}_2(t)=\theta_2(t)-\pi t/T$ for a four-link swimmer ($M=2$) using the first $N=80$ Fourier modes is shown, along with the body configuration at times $t/T=0.2$, $t/T=0.5$, and $t/T=0.8$. The resulting efficiency is $\mathcal{E}=0.0210$, a 28% increase in efficiency over the two-link (rigid) swimmer. (b) The even-numbered Fourier coefficients for a four-link swimmer are shown on a logarithmic scale; the modes are found to decay as $a_{2,n}\sim n^{-3}$ (inset: linear scale).

ments lead the inner segments for $t\in(0,T/2)$, while the opposite is true for $t\in(T/2,T)$. The drag anisotropy of slender filaments is utilized by this more "flexible" body as it increases the surface material, which is presented to the fluid at each stage of the stroke. The consequence is an improved efficiency of $\mathcal{E}=0.0210$, a 28% increase over the two-link swimmer. The optimal stroke is found to be symmetric about the half-period, $t=T/2$, with $a_{2,n}=0$ for n odd. This symmetry is not assumed *a priori*, but is the result of the numerical optimization. The (even-numbered) Fourier modes $a_{2,n}$ are presented in Fig. 2(b). The modes decay like $a_{2,n}\sim n^{-3}$, implying that the angle $\theta_2(t)$ limits as $N\to\infty$ to a function which is twice, but not many times differentiable.

By introducing more links, the optimized stroke form becomes even more efficient, and the body begins to resemble two smooth flagella. The optimal stroke form for an eight-link swimmer ($M=4$) found using the first 40 Fourier modes ($N=40$) is shown in the first panel of Fig. 3. In an extension of the dynamics exhibited by the four-link swimmer, the segments near the free ends are able to present more surface material to the fluid both earlier and later in the stroke than the two-link rigid body. The corresponding efficiency is $\mathcal{E}=0.0268$, a 63% improvement over the two-link swimmer. The deviation angles for the eight-link ($M=4$) swimmer are shown in Fig. 4(a). As expected, the end segments ($k=M$) are found to experience the largest deviation from the rigid dynamics. However, the second angle $\theta_2(t)$ is observed to undergo an unexpected deviation from rigid motion; the curvature at the second joints ($k=2$) are opposite in sign to the curvature on the rest of the flagellar lengths for the bulk of the stroke. In order to better explain this puzzling cavity, we proceed to consider even more flexible bodies.

The second and third panels of Fig. 3 show the optimal 20-link ($\mathcal{E}=0.0363$) and 48-link ($\mathcal{E}=0.0426$) stroke forms, as determined for $N=40$ Fourier modes. The added flexibility not only allows for the presentation of more material to the

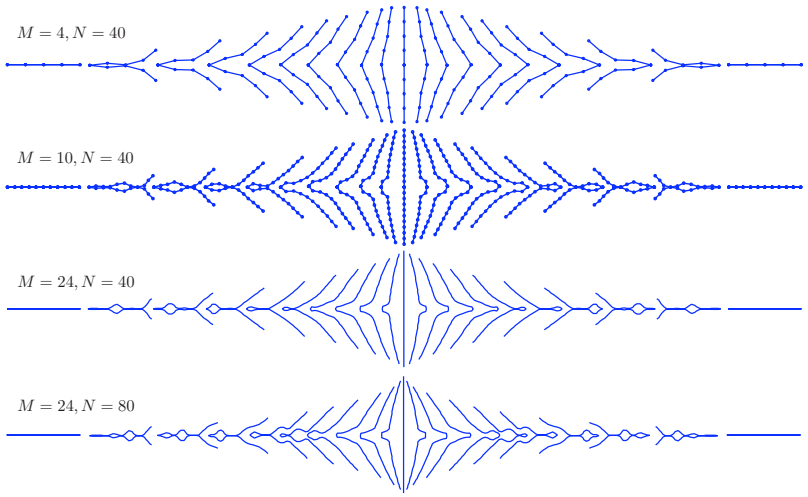

FIG. 3. (Color online) Stroke forms of the optimal eight-link, 20-link, and 48-link swimmers are shown at equally spaced times in $t/T\in[0,1]$ (in multiples of $t/T=0.05$). Solutions are determined using the number of Fourier modes N as indicated. Increasing flexibility not only allows the body to present more material to the fluid, but also allows for the passage of waves down along the body length at the beginning and end of the stroke. (The actual distance traveled is not depicted.)

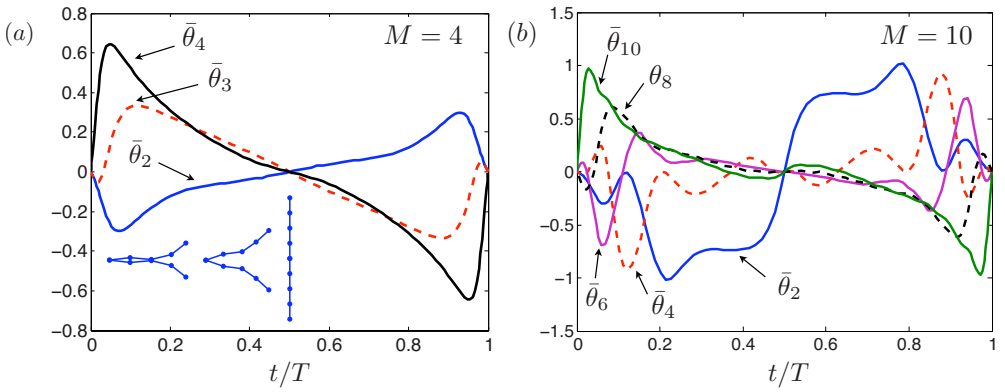

FIG. 4. (Color online) The deviation angles are presented for the eight-link (a) and 20-link (b) cases $[\bar{\theta}_k(t)=\theta_k(t)-\pi t/T]$. An unexpected cavity in the first case is made more clear in the second: the passage of a wave from the tail toward the hinge is observed in the more flexible body for $t/T \in (0,0.2)$, and in the opposite direction for $t/T \in (0.8,1)$.

fluid, but in fact allows for the passage of waves down along the body length during the early and late stages of the stroke. At early times the end segments begin to "unzip" while simultaneously a small protrusion develops on the body's inner segments. The protrusion moves from the flagellar ends toward the hinge during the early part of the stroke, and from the hinge toward the ends during the final part of the stroke. Both waves move to the left, and therefore both generate a swimming motion to the right [29]. The unexpected curvature variation observed in the $M=4$ case is hence explained as the early development of wavelike dynamics for semiflexible biflagellar locomotion.

The deviation angles for the 20-link ($M=10$) swimmer are shown in Fig. 4(b). The unzipping of the end segments as the stroke begins is seen here as a wave traveling from the last deviation angle $\bar{\theta}_{10}$ toward the inner segments for $t/T \in (0,0.2)$. Simultaneously, a second wave of opposite sign is also seen passing toward the inner segments, beginning with a small negative deviation in $\bar{\theta}_8$. This second wave corresponds to the protrusion wave discussed above. The opposite waves are exhibited near the end of the stroke from $t/T \in (0.8,1)$.

If the number of Fourier modes N is increased, the body can express behavior even closer to that of an undulating filament. The fourth panel of Fig. 3 shows the optimal swimmer again for the 48-link body, but now using the first $N=80$ Fourier modes. A second protrusion wave beyond that seen in the $N=40$ case is apparent at early times, and in fact a third wave communicates with the already unzipped parts of the body which propagate toward the left. With the body taking on more wavelike dynamics with increasing flexibility, we are led to the result that there is a degeneracy in the limit of infinite flexibility ($M,N\to\infty$). The hydrodynamically optimal infinitely flexible rehinging swimmer takes on the dynamics of two undulating slender filaments, as illustrated in Fig. 5(a). At zero Reynolds number, with time entering into the dynamics only as a parameter, the body can pass undulatory waves along the two filaments S_i at arbitrarily large speeds compared to the fundamental motion of the innermost angle. With the exception of an arbitrarily short time where the body reorients from ends-right to ends-left, the optimal swimmer behaves no different than an infinite swimming filament as presented by Lighthill, which for planar waves takes the shape of a sawtoothed wave with tangent angle everywhere approximately equal to 40° [24]. Thus an upper bound on the efficiency of rehinging locomotion is that of the infinite undulating filament, $\mathcal{E}=0.086$, or 520% of the two-link rigid rehinging swimmer. Moreover, degenerate solutions are also expected for $N\to\infty$ and $M \geq 3$ (finite). For example in the $M=3$ case, with no other constraints on the relative speeds of angular motions, the last two links on each filament can undergo power and recovery strokes infinitely many times before the first link has com-

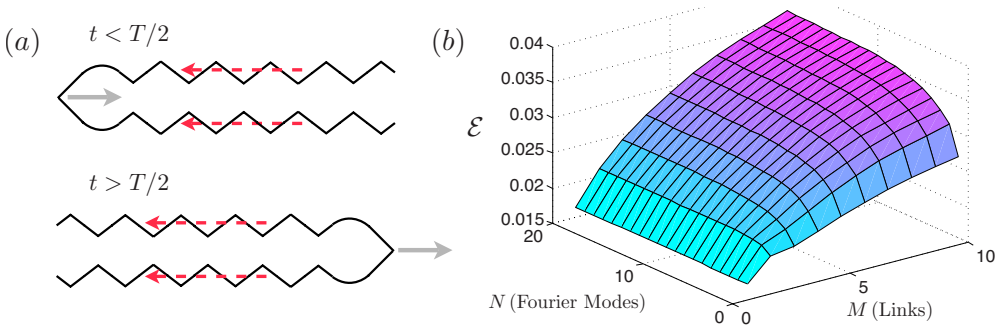

FIG. 5. (Color online) (a) The degenerate infinitely flexible solution: the body takes on the morphology of a pair of undulating slender filaments with wave speeds much faster than the rotating motion of the innermost angle. The optimal infinitely flexible planar waves are sawtoothed with tangent angle everywhere equal to approximately 40° [24]. Arrows with dashed lines indicate wave direction, arrows with solid lines the net swimming direction. (b) The efficiency $\mathcal{E}$ is shown as a function of the number of links M and Fourier modes N.

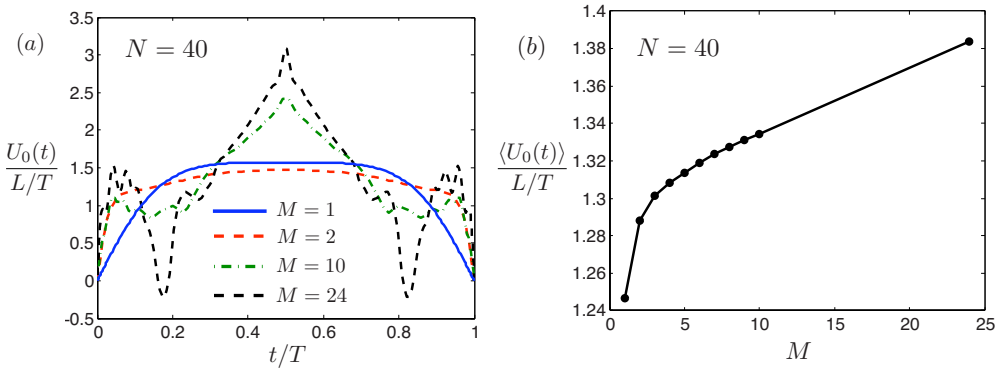

FIG. 6. (Color online) (a) The hinge velocity profiles are shown for a selection of segment numbers M, using $N=40$ Fourier modes. (b) The mean hinge velocity as a function of segment numbers.

pleted its rotation (see [30]). The four-link body ($M=2$) is too rigid to express such dynamics; at each time t there are no possible (infinitely fast) motions by the second link on each filament, which result in a net swimming motion. This degeneracy in the limit of infinite flexibility is considered more directly by Spagnolie and Lauga [31].

Figure 5(b) shows the efficiency $\mathcal{E}$ of the semiflexible rehinging body as a function of the number of links and the Fourier modes. The efficiency increases for both increased M and N, as expected. (A more flexible body can always "choose" to swim like a more rigid body, assuming the joint locations on the former include those on the latter.) In each dimension there are apparently diminishing returns, at least for relatively small M, N: we find that dramatic efficiency gains by the addition of flexibility are achieved early on, and that further increases in the number of degrees of freedom increase the propulsive efficiency at a decreasing rate. Figure 5(b) indicates that the addition of more links is more important than the number of modes of angular motion in this regime. These results may be encouraging for those wishing to design such swimmers; large gains can be achieved through relatively small adjustments to the two-link rigid rehinging swimmer.

Figure 6(a) shows the velocity of the connecting hinge for a selection of link numbers M, found using $N=40$ Fourier modes. The hinge velocity is largest when the body is presenting its largest surface area to the fluid at the half-period, as can be seen in Fig. 3. The rest of the body acts as a wall as the hinge passes through to the right, and the inner protrusion waves begins to develop while the end segments undergo the remaining part of the flexible stroke. In the limit of infinite flexibility the wall is infinitely longer than the smallest deformable body segment, so that the degenerate limit the hinge can pass through with unbounded relative velocity. The hinge velocity at the half-period $t=T/2$ is not quite monotonic in the number of links. The hinge of the four-link body ($M=2$) moves faster during the early and late stages of the stroke, but slower at the half-period than in the two-link rigid case ($M=1$). However, there is a general trend toward increasing hinge velocities at the half-period past a small number of segments.

The connecting hinge does not move unidirectionally in every case. The hinge actually moves opposite the direction of net motion for short times in the optimal 48-link body at approximately $t/T=0.2$ and $t/T=0.8$, when the inner protrusion wave reaches the hinge, and again later when the final protrusion wave is just beginning to develop (see Fig. 3). Figure 6(b) shows the mean hinge velocity over one period. The mean velocity increases dramatically as the number of segments on each filament increases from $M=1$ to $M=5$, and then for $M>5$ appears to grow linearly to at least $M=24$, the largest number of segments considered. It is possible that this apparently linear growth may persist for $M\gg 1$; given the degeneracy described above, there is no lower bound on either the maximal or mean hinge velocities in the limit as M, $N\to\infty$.

IV. CONCLUDING REMARKS

A means of swimming through a viscous fluid, rehinging locomotion, has been introduced. The simplest, rigid case is found to perform on par with more complex forms of locomotion, with an efficiency similar to the optimized three-link swimmer of Purcell [1]. We have shown that the hydrodynamic efficiency can be increased dramatically by increasing the degrees of freedom in an analogous flexible system, and that the optimal stroke form for semiflexible bodies involves the onset of wavelike dynamics along the inner flagellar segments. An upper bound on the efficiency is set by the degenerate solution of two undulating filaments in the limit of infinite flexibility.

In any real manifestation of flexible rehinging locomotion, the degeneracy in the model presented here will be removed by many possible physical considerations. For example, we have neglected energetic costs associated with the bending of the filaments, which are shown by Spagnolie and Lauga [31] to remove a similar degeneracy in the swimming of a single slender filament. In addition, the low Reynolds number assumption breaks down as the undulatory waves increase in speed, presenting another potential mollification of the degeneracy in practical application.

The assumption of the applicability of resistive force theory allowed for a simple analysis, but could be improved upon significantly. The slender body theory of Keller and Rubinow [32] and Johnson [33] shows that the next order term in the asymptotic expansion for the velocity in terms of the fluid stress is $O(1)$, which is not well separated from the $O(\ln(\epsilon))$ term in the resistive force theory for bodies of all

but vanishing aspect ratio. In addition, resistive force theory is certain to break down at the early and late stages of the stroke considered here, when the upper and lower filaments S_i are in near contact. For very flexible bodies ($M \gg 1$), errors so introduced are likely even more pronounced. However, for more rigid bodies the time window most relevant to the propulsion is near the half-period of the stroke, so the possible errors made during the early and late stages may not be as detrimental to the results in these cases.

Finally, we note that the two-dimensional rehinging motion discussed here may be recovered in three dimensions with a round flexible filament. A loop pulled tight to an ellipse with ellipticity ≈ 1 that hinges around a "joint" in the center approximates the 2D motion as discussed. Then, after one such stroke, another 2D stroke is obtained by rotating in the plane perpendicular to that of the first. Rehinging is unnecessary in this case; the active pivot point of rotation on the body acts as the hinge in the two-dimensional case.

ACKNOWLEDGMENTS

The author thanks S. Childress, M. Shelley, and E. Lauga for helpful discussions, and thanks the first-named for suggesting the "rehinging" loop mechanism discussed in the conclusion.

[1] E. M. Purcell, Am. J. Phys. **45**, 3 (1977).
[2] S. Childress and R. Dudley, J. Fluid Mech. **498**, 257 (2004).
[3] N. Vandenberghe, J. Zhang, and S. Childress, J. Fluid Mech. **506**, 147 (2004).
[4] S. Alben and M. Shelley, Proc. Natl. Acad. Sci. U.S.A. **102**, 11163 (2005).
[5] J. Lighthill, SIAM Rev. **18**, 161 (1976).
[6] C. Brennen and H. Winet, Annu. Rev. Fluid Mech. **9**, 339 (1977).
[7] E. Lauga and T. R. Powers, Rep. Prog. Phys. **72**, 096601 (2009).
[8] S. M. Block, K. A. Fahrner, and H. C. Berg, J. Bacteriol. **173**, 933 (1991).
[9] L. Turner, W. S. Ryu, and H. C. Berg, J. Bacteriol. **182**, 2793 (2000).
[10] K. Drescher, K. C. Leptos, and R. E. Goldstein, Rev. Sci. Instrum. **80**, 014301 (2009).
[11] R. A. Freitas, Jr., *Nanomedicine, Volume I: Basic Capabilities* (Landes Bioscience, Georgetown, 1999).
[12] R. Dreyfus, J. Baudry, M. L. Roper, M. Fermigier, H. A. Stone, and J. Bibette, Nature (London) **437**, 862 (2005).
[13] T. S. Yu, E. Lauga, and A. E. Hosoi, Phys. Fluids **18**, 091701 (2006).
[14] B. Behkam and M. Sitti, Appl. Phys. Lett. **90**, 023902 (2007).
[15] M. Roper, R. Dreyfus, J. Baudry, M. Fermigier, J. Bibette, and H. A. Stone, Proc. R. Soc. London, Ser. A **464**, 877 (2008).
[16] J. E. Avron, O. Kenneth, and D. H. Oaknin, New J. Phys. **7**, 234 (2005).
[17] J. E. Avron, O. Gat, and O. Kenneth, Phys. Rev. Lett. **93**, 186001 (2004).
[18] M. Kulić, R. Thaokar, and H. Schiessel, Europhys. Lett. **72**, 527 (2005).
[19] A. M. Leshansky and O. Kenneth, Phys. Fluids **20**, 063104 (2008).
[20] A. M. Leshansky, O. Kenneth, O. Gat, and J. E. Avron, New J. Phys. **9**, 145 (2007).
[21] S. Jung, S. E. Spagnolie, K. Parikh, M. Shelley, and A.-K. Tornberg, Phys. Rev. E **74**, 035302(R) (2006).
[22] J. Gray and G. J. Hancock, J. Exp. Biol. **32**, 802 (1955).
[23] L. E. Becker, S. A. Koehler, and H. A. Stone, J. Fluid Mech. **490**, 15 (2003).
[24] J. Lighthill, *Mathematical Biofluiddynamics* (SIAM, Philadelphia, 1975).
[25] S. Childress, *Mechanics of Swimming and Flying* (Cambridge University Press, Cambridge, U.K., 1981).
[26] D. Tam and A. E. Hosoi, Phys. Rev. Lett. **98**, 068105 (2007).
[27] K. E. Atkinson, *An Introduction to Numerical Analysis* (Wiley, New York, 1978).
[28] O. Raz and J. E. Avron, Phys. Rev. Lett. **100**, 029801 (2008).
[29] G. Taylor, Proc. R. Soc. London, Ser. A **209**, 447 (1951).
[30] J. Blake, J. Fluid Mech. **55**, 1 (1972).
[31] S. Spagnolie and E. Lauga, e-print arXiv:0909.4826.
[32] J. B. Keller and S. I. Rubinow, Biophys. J. **16**, 151 (1976).
[33] R. E. Johnson, J. Fluid Mech. **99**, 411 (1980).